Synthesis and structural refinement of isomorphic cyclosilicate Ca3RE2(Si3O9)2 (RE = Nd, Sm, Gd, Dy, Yb)

François Perrudin, Carine Petitjean, Pierre-Jean Panteix, Florian Brix, Justine Bonnal, David Bonina, Michel Vilasi

Version of Record: https://www.sciencedirect.com/science/article/pii/S0022459622004376
Manuscript_1a4cb77274ef0fa2026a2232cb41d39f

Synthesis and structural refinement of isomorphic cyclosilicate $Ca_3RE_2(Si_3O_9)_2$ (RE = Nd, Sm, Gd, Dy, Yb)

François Perrudin[a], Carine Petitjean[b], Pierre-Jean Panteix[b*], Florian Brix[c], Justine Bonnal[b], David Bonina[b], Michel Vilasi[b]

[a] *CEA, DES, ISEC, DE2D, University of Montpellier, Marcoule, France*
[b] *Université de Lorraine, CNRS, Institut Jean Lamour, F 54011 Nancy, France*
[c] *Center for Interstellar Catalysis, Department of Physics and Astronomy, Aarhus University, Ny Munkegade 120, Aarhus C 8000, Denmark*

[*]corresponding author
e-mail: pierre-jean.panteix@univ-lorraine.fr

Abstract

The introduction of rare earth elements in protecting coatings against degradation due to chemical interactions with liquid silicates as CMAS (CaO-MgO-Al_2O_3-SiO_2) is very promising. They lead to the precipitation of several silicates, as cyclosilicate and apatite phases. In this work, rare earth cyclosilicate phases with formula $Ca_3RE_2(Si_3O_9)_2$ (RE = Nd, Sm, Gd, Dy, Yb) and space group C2/c have been prepared by solid state reaction at 1400°C. High purity powders (with few percents of apatite as impurity) have been obtained. XRD characterization has been performed via synchrotron and the patterns were refined by Rietveld method. Considering that the ionic radius of Ca^{2+} is larger than the ionic radius of all the RE^{3+} studied here, the repartition of both cations in the three cationic sites of the structure has been specifically observed. In all cases, the three sites can be occupied by both Ca^{2+} and RE^{3+}, and the repartitions depend on the ionic radius of RE^{3+}.

Keywords

crystal structure; powder diffraction; cyclosilicate; rare earth; coordination.

1. Introduction

In order to increase the efficiency of aeronautical engines and to decrease their environmental impact, new materials and coatings must be developed. Thermal and environmental barrier coatings (i.e. E/TBCs) added with different rare earth elements are promising. They are subject to degradation by contact with molten siliceous deposits resulting from the ingestion of mineral particles. These deposits are mainly constituted of CaO, MgO, Al_2O_3 and SiO_2 (i.e. CMAS). Recent works by [1-5] have shown that E/TBC compositions containing rare earths can lead to reactions with the silicate melt and result in the formation of precipitated silicates, e.g. apatite and cyclosilicate. Few thermodynamic data are available in these systems. Poerschke et al. [6-8] have reported diagrams in the Y_2O_3-CaO-SiO_2 and Gd_2O_3-CaO-SiO_2 systems at 1400°C and 1600°C, highlighting the existence of the RE-cyclosilicate phases $Ca_2RE_2(Si_3O_9)_2$ in equilibrium with the melt.

The crystal structure of yttrium cyclosilicate $Ca_3Y_2(Si_3O_9)_2$ has already been reported by Yamane et al. [9]. It is derived from the structure of pseudo-wollastonite α-$CaSiO_3$ and crystallizes in space group C2/c, with Z = 4 [10,11]. Many substitutions are possible in the cyclosilicate structure: for example, cationic sites can be occupied by both ME^{2+} and RE^{3+} cations. Ca can be substituted by other alkaline earths as Sr [12], and Y has already been substituted by many rare earths (Eu-Lu) in order to study luminescence properties [12,13]. There are three types of cationic sites, with different coordination numbers: $(Ca/RE)_1$ sites, $(Ca/RE)_2$ sites and $(Ca/RE)_3$ sites are surrounded by eight, seven and six oxygen atoms respectively. There are twice more $(Ca/RE)_1$ and $(Ca/RE)_2$ sites (Wyckoff notation 8f) than $(Ca/RE)_3$ sites (Wyckoff notation 4e). The aim of this paper is to study the influence of the nature of the rare earth on the occupancy of the three cationic sites of the cyclosilicate structure. Different rare earth cyclosilicates $Ca_3RE_2(Si_3O_9)_2$ (with RE = Nd, Sm, Gd, Dy and Yb) have been prepared by solid state reaction at 1400°C. The chosen rare earths have ionic radii lower than Ca see Table 1. The crystallographic structures of the different rare earth cyclosilicates have been determined after XRD characterization performed on synchrotron and Rietveld refinement of the acquired patterns.

2. Materials and methods

2.1 Powders synthesis

A set of five compounds with $Ca_3RE_2(Si_3O_9)_2$ composition, RE = Nd, Sm, Gd, Dy, Yb, was elaborated by solid state synthesis from adequate amounts of $CaCO_3$ (99%, Prolabo), amorphous SiO_2 (99.9%, Aldrich) and lanthanide sesquioxides RE_2O_3 powder reagents. All rare earth oxide powders, provided by Treibacher Industrie AG and Cerac, were highly pure (> 99.5%). The mixtures were finely grounded in agate mortar and then calcinated twice at 1400°C for 6h (heating/cooling rate of 180°C/h) with an intermediate grinding. A $Pt_{95}Au_5$ crucible was used to avoid any concomitant reaction. To remove eventual unreacted rare earth oxides, the resulting powders were washed by nitric acid solution followed by vacuum filtration [15].

2.2 Powders characterization

The synthetic cyclosilicate powders were dispersed and embedded in epoxy resin for Scanning Electron Microscope (SEM) (LEO Gemini DSM982 high resolution field-emission gun) observation operating at 10 kV. The surface of samples was preliminarly polished (¼ µm, diamond stick) and coated by a thin layer of carbon. Phase homogeneity was then verified using Back Scattered Electron (BSE) imaging mode, and the synthesis impurities were identified by Energy Dispersive X-ray Spectroscopy (EDS, Kevex Quantum type).

The surface fraction of Gd-apatite phase (main synthesis impurity) in $Ca_3Gd_2(Si_3O_9)_2$ powder was extracted by quantitative image analysis with the Aphelion® software. A set of 15 high-resolution (2000 × 2000 pixels) SEM images within a 185 µm² observation area (magnification × 500) was first captured in BSE chemical contrast mode. The two Gd-apatite and Gd-cyclosilicate phases were then segmented in the micrographs thresholding manually grey values, and the respective areas were measured in the binary images. These data were used to calculate the area covered by the Gd-apatite phase which is divided by the total crystalized area: $\%F = \%F_{Ap} / (\%F_{Ap} + \%F_{Cy})$.

Powder X-Ray Diffraction (XRD) experiments of cyclosilicate compounds were performed using the CRISTAL beamline of the SOLEIL synchrotron facility (Paris, France). Each sample was introduced in a quartz capillary (0.3 mm of diameter) spinning around its axis to reduce preferred orientation (PO) of the crystallites. All the patterns were collected in transmission using a Debye-Scherrer geometry using a monochromatic X-ray source set at λ =

0.72930 Å (beam energy 17 keV). Data were recorded at room temperature with a 21 silicon (111) monocrystal analyser in the angular range $0° \leq 2\theta \leq 60°$ with a step of 0.002°.

The Rietveld method was employed for the crystal structure refinement of cyclosilicate phases using the Fullprof program and the previous XRD data. For the first refinement with $Ca_3Yb_2(Si_3O_9)_2$, the monoclinic $Ca_3Y_2(Si_3O_9)_2$ phase (space group C2/c) [9] was selected as the original structure model in which the scattering factor of Yb^{3+} replaced the Y^{3+} one. Then, the output structure data (lattice parameters, atomic position, occupancy factors …) were recursively used as the new starting point for next refinement of $Ca_3RE_2(Si_3O_9)_2$ (Yb → Dy → Gd → Sm → Nd).

For all RE-cyclosilicates, the background was fitted with a six-order polynomial function and the peak profile was modelled using a pseudo-Voigt function. The same refinement strategy (~ 64 parameters) was applied with no geometric restraints (bond length and bond angle) and the refined parameters obtained after each cycle were imported in the input file for next step. (i) Some parameters such as the flat background, the lattice parameters or the scale factor were first manually adjusted. (ii) Refinement of the scale factor, the flat background coefficient and the zero shift parameter. (iii) Refinement of the lattice parameters. (iv) Refinement of the five remaining background coefficients. (v) Refinement of the W, U and V parameters of the Caglioti function $FWHM = (U \tan^2 \theta + V \tan \theta + W)^{1/2}$ which describes the Full line width at Half Maximum of the peak. (vi) Refinement of the peak shape function which distributes the Gaussian and Lorentzian part in the pseudo-Voigt profile $I(2\theta) = \alpha L(2\theta) + (1-\alpha) G(2\theta)$ and the x parameter which describes the 2θ-dependency of the peak shape function. (vii) Refinement of the overall temperature factor (Bov). (viii) Refinement of the fractional atomic position for Ca and RE cations (except special positions (0, y, 1/4) for $(Ca/RE)_3$). (ix) Refinement of the three Ca/RE occupancy sites for which both elements were complementarily refined with opposite shifts. (x) Refinement of the fractional atomic position for Si and then O.

This last procedure (from step (ii) to (v)) was also conducted for the second minor apatite phase when some peaks were available with good definition. It was therefore possible to get a reliable estimate of the percentage of the two different silicate phases.

3. Results

A SEM micrograph (back-scattered electrons) of the synthesized Gd-cyclosilicate powder is presented in Figure 1. Three phase contrast levels are observed, and can be identified thanks to EDS analysis. The predominant phase consists in large grains (from few micrometers to more than 200 µm) with intermediate contrast and correspond to the desired Gd-cyclosilicate $Ca_3Gd_2(Si_3O_9)_2$. The two other phases are located on the surface of these large grains: the needle-shaped bright phase (about 20 µm long) is Gd-apatite $Gd_8Ca_2(SiO_4)_6O_2$, and the darker areas are traces of wollastonite $CaSiO_3$. This latter phase will be neglected in the Rietveld refinements. The surface fraction of Gd-apatite evaluated by image analyses is 5.7 ± 2.1 %.

Figure 2 presents the synchrotron XRD pattern of the synthesized Gd-cyclosilicate powder. A very good agreement is observed with the superimposed Rietveld refinement. The presence of apatite has been taken into account in the refinement, leading to an evaluated proportion of 6.2 % of apatite phase (Table 2). This value is in the range measured by image analyses. For all the RE-cyclosilicates studied here, the reliability factors χ^2_{global}, R_{Bragg}, and $R(F^2)$ are relatively low, which is acceptable considering that the analyses have not been performed on single crystals. Table 2 also includes the obtained CSD numbers of the 5 refined cyclosilicate structures.

The evolution of the unit cell constants a, b, c, and β are reported as a function of the ionic radius of the rare earths studied here (sixfold coordination, i.e. octahedral configuration) in Figure 3. The cell parameters a, b and c increase in coherence with the rare earth ionic radius, as the beta angle decreases. All the atomic positions, the interatomic distances and the bond angles are given in Tables 3, 4 and 5 for all the studied rare earths respectively. The average O-Si-O angle values are systematically very close to 109°, which is coherent with the tetrahedral configuration of Si. The $(Ca/RE)_1$, $(Ca/RE)_2$, and $(Ca/RE)_3$ site occupancies are given in Table 6.

4. Discussion

The distribution of Ca and RE in the sites 1, 2 and 3 of the $Ca_3RE_2(Si_3O_9)_2$ structure given in Table 6 are also presented in Figure 4 for RE = Yb, Dy, Gd, Sm and Nd. The

evolution of the RE/Ca ratio in the three different sites are given in Figure 5 as a function of the ionic radius (CN = VI) of the RE^{3+} cations studied here. As the $(Ca/RE)_1$ sites have the highest coordination in the structure (eightfold coordination), they are thus the more likely to accommodate the larger cations. It can be seen here that $(Ca/RE)_1$ sites are mainly occupied by Ca. The lowest coordination of $(Ca/RE)_3$ sites favors the occupancy of the smaller cations. On these sites, the RE/Ca ratio is systematically higher than 1. The same trends are observed for Y-cyclosilicate in [9]. The increasing difference between the ionic radii of Ca^{2+} and RE^{3+} favors the preferential repartition of the cations on $(Ca/RE)_1$ and $(Ca/RE)_3$ sites. The Ca proportion in $(Ca/RE)_1$ sites is more important when the difference of ionic radius between Ca and RE is great: for example, Ca occupies 89% of $(Ca/RE)_1$ sites in Yb-cyclosilicate, as it occupies only 71% of $(Ca/RE)_1$ sites in Nd-cyclosilicate. Indeed, the Ca proportion in $(Ca/RE)_3$ sites is less important when the difference of ionic radii between Ca and RE is great: 15% in the case of Yb-cyclosilicate and 38% in the case of Nd-cyclosilicate. $(Ca/RE)_2$ sites exhibit an intermediate behavior with an almost constant rare earth occupancy (55-58%).

The Ca-cyclosilicate phase can be compared to the Sr-cyclosilicate (with RE = Y, Eu-Lu) phase investigated by Tyutyunnik et al. [12]. In the case of Ca-cyclosilicate, the evolution of the structure with the rare earth ionic radius exhibits no transition. The lattice parameters increase continuously as for Sr-cyclosilicate, starting from erbium. Data concerning RE-cyclosilicate with Sr are presented in Figure 6 [12]. The ionic radius of Sr^{2+} in sixfold coordination is 118 pm [14], which is larger than Ca^{2+} (100 pm). The evolution of the RE/Sr ratios *vs.* RE^{3+} ionic radii for the three different sites of the structure can thus be compared to the RE/Ca ratios presented in Figure 5, both figures showing the influence of RE on the occupancy of the three sites. In both cases (Ca and Sr), $(Ca/RE)_1$ sites are mostly occupied by Ca, as $(Ca/RE)_3$ sites are mostly occupied by RE. But, in the case of Sr, the RE/Sr ratio show no clear dependence with the RE^{3+} ionic radius. It can be concluded that when the alkaline-earth becomes larger (e.g. increasing from Ca to Sr), the nature of the rare earth has no influence on the Ca/RE repartition in the three sites of the cyclosilicate structure.

5. Conclusion

The synthesis of rare earth cyclosilicates $Ca_3RE_2(Si_3O_9)_2$ (RE = Nd, Sm, Gd, Dy, Yb) by high temperature solid state reactions led to powders containing mainly the desired phase

and a few percent of rare earth oxyapatite as impurity. The Rietveld refinement of the crystal structure of the cyclosilicate phases showed cell parameters coherent with the ionic radius of the substituting rare earths. The repartition of the RE^{3+} and Ca^{2+} cations in the three cationic sites of the structure strongly depends on the coordination of the cationic site. $(Ca/RE)_1$ sites, which has the highest coordination, is always mainly occupied by the largest cation i.e. Ca^{2+}. Conversely, $(Ca/RE)_3$, which has the lowest coordination, is always mainly occupied by RE^{3+}. When the ionic radius of RE^{3+} increases, their occupancy increases on $(Ca/RE)_1$ sites and decreases on $(Ca/RE)_3$ sites.

Acknowledgment

The experiments were performed on the Cristal Beamline at Synchrotron SOLEIL, France (Proposal No. 20160294). The authors acknowledge Erik Elkaïm for the data acquisition.
The authors would like to acknowledge DGA and ONERA for the financial support.

References

[1] J. Liu, L. Zhang, Q. Liu, L. Cheng, Y. Wang, Calcium-magnesium-aluminosilicate corrosion behaviors of rare-earthh disilicates at 1400°C (2013), J. Eur. Ceram. Soc. 33 (2013) 3419-3428. http://dx.doi.org/10.1016/j.jeurceramsoc.2013.05.030.

[2] F. Perrudin, C. Rio, M.H. Vidal-Setif, C. Petitjean, P.J. Panteix, M. Vilasi, Gadolinium oxide solubility in molten silicate: dissolution mechanismand stability of $Ca_2Gd_8(SiO_4)_6O_2$ and $Ca_3Gd_2(Si_3O_9)_2$ silicate phases, J. Eur. Ceram. Soc. 37 (2017) 2657-2665. http://dx.doi.org/10.1016/j.jeurceramsoc.2017.02.022.

[3] F. Perrudin, M.H. Vidal-Setif, C. Rio, C. Petitjean, P.J. Panteix, M. Vilasi, Influence of rare earth oxides on kinetics and reaction mechanisms in CMAS silicate melts, J. Eur. Ceram. Soc. 37 (2019) 4223-4232. https://doi.org/10.1016/j.jeurceramsoc.2019.06.036.

[4] Y. Dong, K. Ren, Q. Wang, G. Shao, Y. Wang, Interaction of multicomponent disilicate $(Yb_{0.2}Y_{0.2}Lu_{0.2}Sc_{0.2}Gd_{0.2})_2Si_2O_7$ with molten calcia-magnesia-aluminosilicate, J. Adv. Ceram. 11 (2022) 66-74. https://doi.org/10.1007/s40145-021-0517-7.

[5] V.L. Wiesner, B.J. Harder, A. Garg, N.P. Bansal, Molten calcium–magnesium–aluminosilicate interactions with ytterbium disilicate environmental barrier coating, J. Mater. Res. 35 (2020) 2346-2357. https://doi.org/10.1557/jmr.2020.211.

[6] D.L. Poerschke, T.L Barth, C.G. Levi, Equilibrium relationships between thermal barrier oxides and silicate melts, Acta Mater. (2016) 120, 302-314. http://dx.doi.org/10.1016/j.actamat.2016.08.077.

[7] D.L. Poerschke, T.L. Barth, O. Fabrichnaya, C.G. Levi, Phase equilibria and crystal chemistry in the calcia–silica–yttria system, J. Eur. Ceram. Soc. 36 (2016) 1743-1754. http://dx.doi.org/10.1016/j.jeurceramsoc.2016.01.046.

[8] D.L. Poerschke, C.G. Levi, Phase equilibria in the calcia-gadolinia-silica system, J. Alloy. Cmpd. 695 (2017) 1397-1404. http://dx.doi.org/10.1016/j.jallcom.2016.10.263.

[9] H. Yamane, T. Nagasawa, M. Shimada, T. Endo, $Ca_3Y_2(Si_3O_9)_2$, Acta Cryst. C53 (1997) 1533-1536.

[10] T. Yamanaka, H. Mori, The structure of polytypes of α-$CaSiO_3$ (pseudowollastonite), Acta Cryst. B37 (1981) 1010-1017.

[11] H. Yang, C.T. Prewitt, On the crystal structure of pseudowollastonite ($CaSiO_3$), Am. Mineral. 84 (1999) 929-932.

[12] A.P. Tyutyunnik, I.I. Leonidov, L.L Surat, I.F. Berger, V.G. Zubkov, Crystal structure, morphotropic phase transition and luminescence in the new cyclosilicates $Sr_3R_2(Si_3O_9)_2$, R=Y, Eu–Lu, J. Eur. Ceram. Soc. 197 (2013) 447-455. http://dx.doi.org/10.1016/j.jssc.2012.09.009.

[13] A. Dobrowolska, E. Zych, Luminescence of Tb-doped $Ca_3Y_2(Si_3O_9)_2$ oxide upon UV and VUV synchrotron radiation excitation, J. Solid State Chem. 184 (2011) 1707-1714. https://doi.org/10.1016/j.jssc.2011.05.014.

[14] R.D. Shannon, Revised effective ionic radii and systematic studies of interatomic distances in halides an chalcogenides, Acta Cryst. A32 (1976) 751-767.

[15] P.J. Panteix, I. Julien, D. Bernache-Assollant, P. Abélard, Synthesis and characterization of oxide ions conductors with the apatite structure for intermediate temperature SOFC, Mater. Chem. Phys. 95 (2005) 313-320. https://doi.org/10.1016/j.matchemphys.2005.06.040.

Figure captions

Figure 1. SEM micrograph of the as-elaborated Gd-cyclosilicate powder. Insert: some $CaSiO_3$ and $Ca_2Gd_8(SiO_4)_6O_2$ (Ap) phase impurities found in the sample.

Figure 2. Synchrotron collected XRD pattern (red solid line), Rietveld refinement (black solid line), hkl reflections (green vertical tick lines) and residuals (blue solid line) of $Ca_3Gd_2(Si_3O_9)_2$ ($\chi^2_{global} = 4.87$; $R_{Bragg} = 7.02$; $R(F^2) = 4.26$).

Figure 3. Evolution of the unit cell constants a, b, c and β for $Ca_3RE_2(Si_3O_9)_2$ as a function of the rare earth (RE= Yb, Dy, Gd, Sm, Nd) ionic radius in sixfold coordination.

Figure 4. Cation distribution (%) of Ca and RE (Yb, Dy, Gd, Sm, Nd) in sites 1, 2 and 3 of $Ca_3RE_2(Si_3O_9)_2$.

Figure 5. Evolution of RE/Ca ratio in sites 1, 2 and 3 of $Ca_3RE_2(Si_3O_9)_2$ as a function of the rare earth (RE= Yb, Dy, Gd, Sm, Nd) ionic radius in sixfold coordination.

Figure 6. Evolution of RE/Sr ratio in sites 1, 2 and 3 of $Sr_3RE_2(Si_3O_9)_2$ as a function of the rare earth (RE= Yb, Dy, Gd, Sm, Nd) ionic radius in sixfold coordination [14].

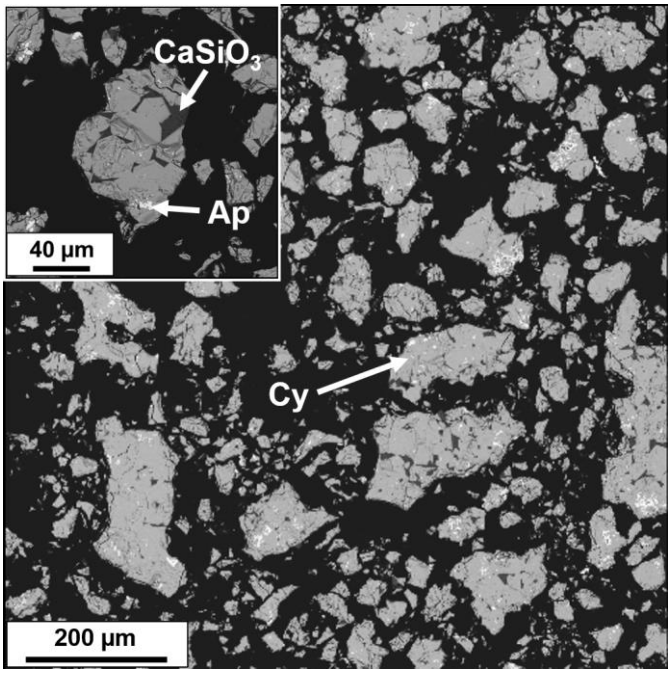
CaSiO3
Ap
40 µm
Cy
200 µm

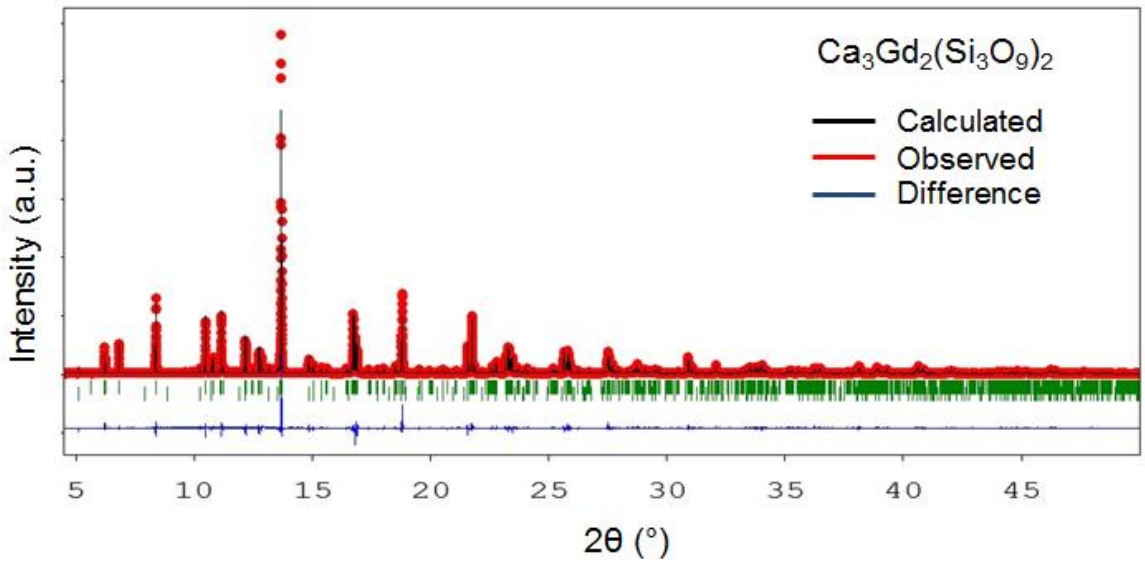
Ca3Gd2(Si3O9)2
Calculated
Observed
Difference
Intensity (a.u.)
5
10
15
20
25
30
35
40
45
2θ (°)

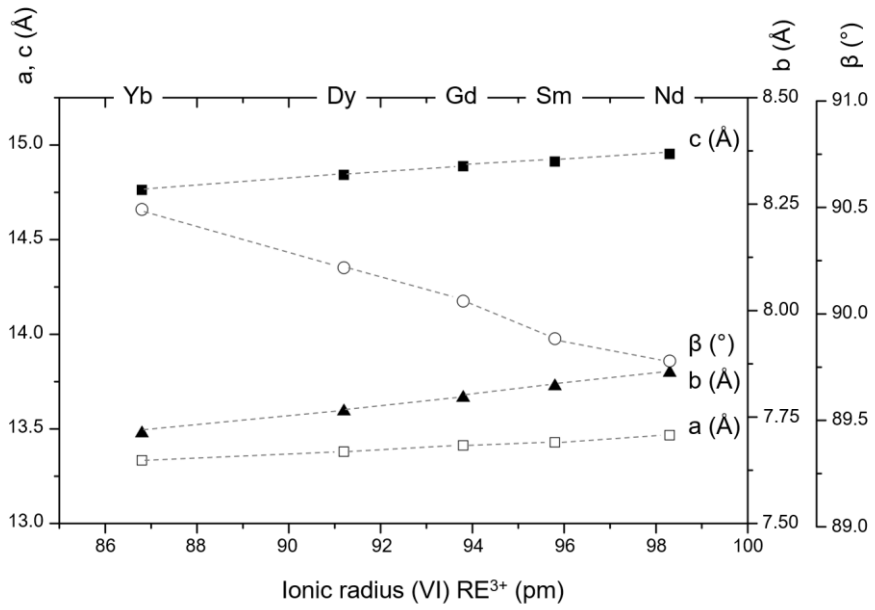
a, c (Å)
b (Å)
β (°)
Yb
Dy
Gd
Sm
Nd
c (Å)
β (°)
b (Å)
a (Å)
15.0
14.5
14.0
13.5
13.0
8.50
8.25
8.00
7.75
7.50
91.0
90.5
90.0
89.5
89.0
86
88
90
92
94
96
98
100
Ionic radius (VI) RE3+ (pm)

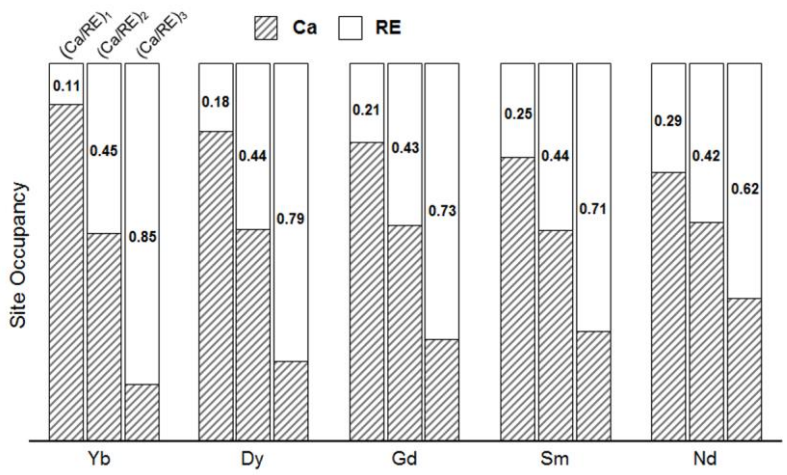
(Ca/RE)1
(Ca/RE)2
(Ca/RE)3
Ca
RE
Site Occupancy
0.11
0.45
0.85
0.18
0.44
0.79
0.21
0.43
0.73
0.25
0.44
0.71
0.29
0.42
0.62
Yb
Dy
Gd
Sm
Nd

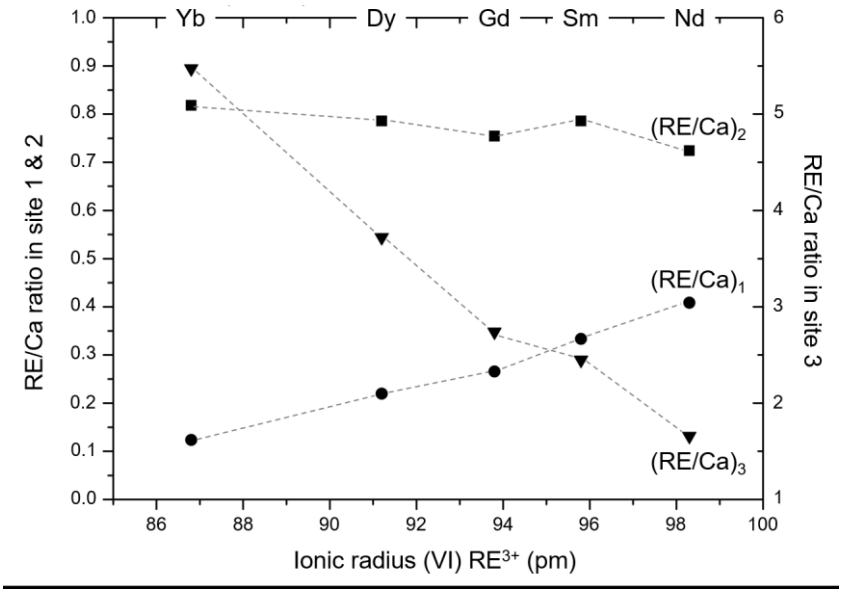
Yb
Dy
Gd
Sm
Nd
(RE/Ca)2
(RE/Ca)1
(RE/Ca)3
RE/Ca ratio in site 1 & 2
RE/Ca ratio in site 3
Ionic radius (VI) RE3+ (pm)
1.0
0.9
0.8
0.7
0.6
0.5
0.4
0.3
0.2
0.1
0.0
6
5
4
3
2
1
86
88
90
92
94
96
98
100

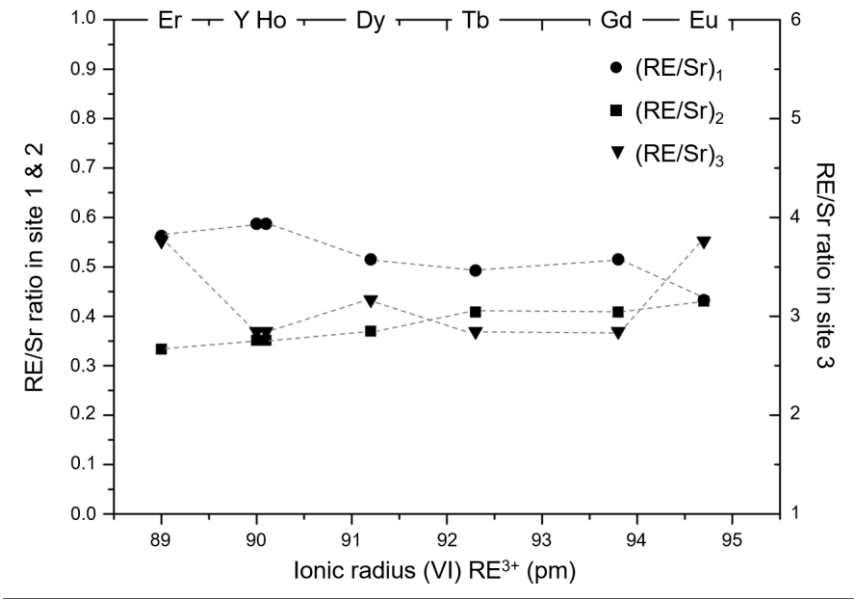
Er
Y Ho
Dy
Tb
Gd
Eu
(RE/Sr)1
(RE/Sr)2
(RE/Sr)3
RE/Sr ratio in site 1 & 2
RE/Sr ratio in site 3
Ionic radius (VI) RE3+ (pm)
1.0
0.9
0.8
0.7
0.6
0.5
0.4
0.3
0.2
0.1
0.0
6
5
4
3
2
1
89
90
91
92
93
94
95

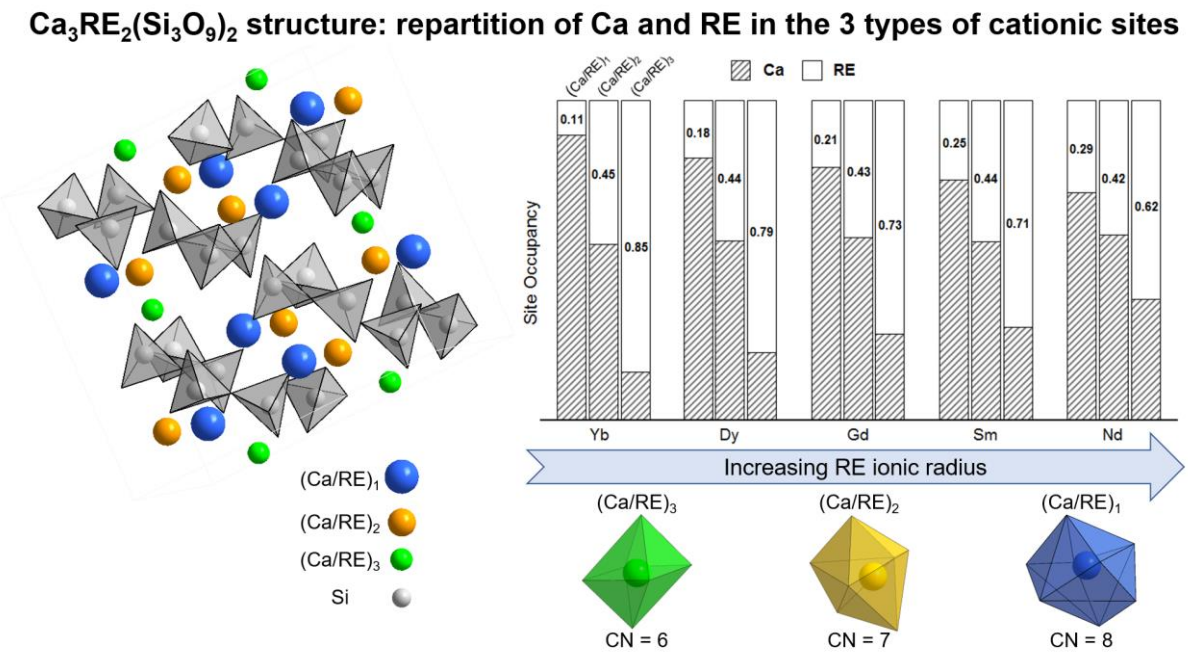

GRAPHICAL ABSTRACT

Table 1. Ionic radius of different rare earth cations RE^{3+} compared to Ca^{2+} (sixfold coordination) [14].

	Yb^{3+}	Y^{3+}	Dy^{3+}	Gd^{3+}	Sm^{3+}	Nd^{3+}	Ca^{2+}
ionic radius (pm)	87	90	91	94	96	98	100

Table 2. Rietveld refinement results of $Ca_3RE_2(Si_3O_9)_2$ (RE= Yb, Dy, Gd, Sm, Nd) compounds.

$Ca_3RE_2(Si_3O_9)_2$		Yb	Dy	Gd	Sm	Nd
Obtained CSD number		2176354	2176346	2176348	2176352	2176350
Refined parameters						
Cell parameters	a (Å)	13.3333(1)	13.3788(1)	13.4123(0)	13.4284(0)	13.4663(1)
	b (Å)	7.7117(1)	7.7629(1)	7.7950(0)	7.8222(0)	7.8539(1)
	c (Å)	14.7625(1)	14.8418(1)	14.8875(0)	14.9122(0)	14.95261)
	β (°)	90.491(1)	90.217(2)	90.060(0)	89.884(0)	89.779(3)
	V ($Å^3$)	1517.9	1541.4	1556.5	1566.4	1581.4
Volumic mass	D ($g.cm^3$)	4.010	3.905	3.814	3.771	3.651
Impurity	($_{Frac.}$% Ap)	4.5	5.3	6.2	6.0	4.2
Reliability Factors	χ^2_{global}	5.37	2.64	4.87	3.85	5.52
	R_{Bragg}	5.17	4.23	7.02	6.91	6.78
	$R(F^2)$	3.61	2.67	4.26	4.44	4.61

Table 3. Refined fractional atomic coordinates for $Ca_3RE_2(Si_3O_9)_2$ (RE= Yb, Dy, Gd, Sm, Nd).

		Yb	Dy	Gd	Sm	Nd
$(Ca/RE)_1$	x/a	0.1588(3)	0.1636(2)	0.1628(0)	0.1631(0)	0.1625(2)
	y/b	0.1174(11)	0.1185(6)	0.1208(0)	0.1178(0)	0.1163(6)
	z/c	0.4123(28)	0.4123(1)	0.4127(0)	0.4129(0)	0.4118(2)
$(Ca/RE)_2$	x/a	0.3364(2)	0.3341(1)	0.3342(0)	0.3347(0)	0.3355(2)
	y/b	0.1268(7)	0.1265(4)	0.1273(0)	0.1244(0)	0.1235(5)
	z/c	0.0840(1)	0.0845(1)	0.0845(0)	0.0832(0)	0.0837(1)
$(Ca/RE)_3$	x/a	0	0	0	0	0
	y/b	0.3813(3)	0.3796(22)	0.3780(0)	0.3779(0)	0.3785(4)
	z/c	0.2500(0)	0.2500(0)	0.2500(0)	0.2500(0)	0.2500(0)
Si(1)	x/a	0.0916(6)	0.0924(4)	0.0906(0)	0.0933(0)	0.0927(5)
	y/b	0.0745(9)	0.0729(5)	0.0702(0)	0.0737(0)	0.0699(8)
	z/c	0.1017(5)	0.0997(3)	0.1015(0)	0.0996(0)	0.0981(4)
Si(2)	x/a	0.2719(6)	0.2749(3)	0.2771(0)	0.2779(0)	0.2757(4)
	y/b	0.3632(13)	0.3673(8)	0.3725(0)	0.3721(0)	0.3713(13)
	z/c	0.2673(46)	0.2678(3)	0.2695(0)	0.2690(0)	0.2673(4)
Si(3)	x/a	0.4000(7)	0.4031(4)	0.4044(0)	0.4059(0)	0.4039(5)
	y/b	0.1782(9)	0.1779(5)	0.1763(0)	0.1804(0)	0.1794(8)
	z/c	0.4073(6)	0.4062(4)	0.4079(0)	0.4041(0)	0.4011(5)
O(1)	x/a	0.0014(0)	0.0014(0)	0.0014(0)	0.0014(0)	0.0014(0)
	y/b	0.1886(20)	0.1799(11)	0.1808(0)	0.1730(0)	0.1751(16)
	z/c	0.1419(9)	0.1397(6)	0.1398(0)	0.1387(0)	0.1333(7)
O(2)	x/a	0.0657(10)	0.0677(6)	0.0675(0)	0.0685(0)	0.0646(7)
	y/b	0.1298(21)	0.1289(13)	0.1328(0)	0.1280(0)	0.1389(16)
	z/c	0.5553(8)	0.5610(5)	0.5594(0)	0.5690(0)	0.5624(7)
O(3)	x/a	0.1520(13)	0.1536(7)	0.1548(0)	0.1602(0)	0.1645(9)
	y/b	0.3788(25)	0.3762(17)	0.3797(0)	0.3741(0)	0.3785(27)
	z/c	0.2925(9)	0.3019(5)	0.2976(0)	0.3042(0)	0.3118(8)
O(4)	x/a	0.1556(11)	0.1541(7)	0.1559(0)	0.1626(0)	0.1628(9)
	y/b	0.1502(30)	0.1509(18)	0.1496(0)	0.1450(0)	0.1487(24)
	z/c	0.0181(9)	0.0172(6)	0.0181(0)	0.0176(0)	0.0189(7)
O(5)	x/a	0.1861(11)	0.1817(7)	0.1779(0)	0.1714(0)	0.1689(10)
	y/b	0.0395(19)	0.0501(11)	0.0442(0)	0.0454(0)	0.0433(15)
	z/c	0.1758(10)	0.1799(6)	0.1802(0)	0.1830(0)	0.1848(9)
O(6)	x/a	0.3063(11)	0.3058(6)	0.3025(0)	0.3029(0)	0.3005(8)
	y/b	0.3580(23)	0.3640(16)	0.3675(0)	0.3706(0)	0.3652(25)
	z/c	0.1692(9)	0.1686(6)	0.1709(0)	0.1680(0)	0.1688(7)
O(7)	x/a	0.3149(11)	0.3227(7)	0.3220(0)	0.3296(0)	0.3266(10)
	y/b	0.195318)	0.1993(11)	0.2065(0)	0.2031(0)	0.2113(15)
	z/c	0.3250(10)	0.3201(6)	0.3246(0)	0.3206(0)	0.3144(9)
O(8)	x/a	0.3366(11)	0.3390(7)	0.3375(0)	0.3364(0)	0.3379(8)
	y/b	0.1030(29)	0.1129(19)	0.1141(0)	0.1091(0)	0.1148(26)
	z/c	0.4870(9)	0.4886(5)	0.4863(0)	0.4903(0)	0.4883(7)
O(9)	x/a	0.4998(13)	0.5057(8)	0.5047(0)	0.5001(0)	0.5003(10)
	y/b	0.0769(20)	0.0756(12)	0.0800(0)	0.0767(0)	0.0802(16)
	z/c	0.1321(9)	0.1301(5)	0.1310(0)	0.1301(0)	0.1227(7)

Table 4. Selected interatomic distances in $Ca_3RE_2(Si_3O_9)_2$ (RE= Yb, Dy, Gd, Sm, Nd).

Bond (Å)	Yb	Dy	Gd	Sm	Nd
$(Ca/RE)_1 – O(1)$	2.34	2.38	2.38	2.38	2.36
$(Ca/RE)_1 – O(2)$	2.46	2.56	2.53	2.65	2.61
$(Ca/RE)_1 – O(3)$	2.68	2.59	2.65	2.58	2.54
$(Ca/RE)_1 – O(4)$	2.59	2.61	2.63	2.58	2.63
$(Ca/RE)_1 – O(6)$	2.38	2.35	2.38	2.32	2.36
$(Ca/RE)_1 – O(7)$	2.53	2.61	2.59	2.71	2.75
$(Ca/RE)_1 – O(8)$	2.61	2.60	2.59	2.60	2.63
$(Ca/RE)_1 – O(8)$	2.62	2.55	2.56	2.58	2.59
$(Ca/RE)_1 – O$	**2.53**	**2.53**	**2.54**	**2.54**	**2.56**
$(Ca/RE)_2 – O(3)$	2.65	2.58	2.61	2.58	2.58
$(Ca/RE)_2 – O(4)$	2.60	2.61	2.59	2.52	2.53
$(Ca/RE)_2 – O(4)$	2.29	2.30	2.32	2.35	2.36
$(Ca/RE)_2 – O(5)$	2.52	2.56	2.62	2.72	2.77
$(Ca/RE)_2 – O(6)$	2.22	2.26	2.31	2.34	2.33
$(Ca/RE)_2 – O(8)$	2.28	2.34	2.38	2.29	2.35
$(Ca/RE)_2 – O(9)$	2.32	2.42	2.42	2.36	2.32
$(Ca/RE)_2 – O$	**2.41**	**2.44**	**2.46**	**2.45**	**2.46**
$(Ca/RE)_3 – O(1)$	2.18	2.25	2.25	2.31	2.37
$(Ca/RE)_3 – O(1)$	2.18	2.25	2.25	2.31	2.37
$(Ca/RE)_3 – O(3)$	2.12	2.19	2.19	2.30	2.40
$(Ca/RE)_3 – O(3)$	2.12	2.19	2.19	2.30	2.40
$(Ca/RE)_3 – O(9)$	2.30	2.34	2.37	2.37	2.48
$(Ca/RE)_3 – O(9)$	2.30	2.34	2.37	2.37	2.48
$(Ca/RE)_3 – O$	**2.20**	**2.26**	**2.27**	**2.33**	**2.42**
Si(1) – O	**1.67**	**1.65**	**1.66**	**1.63**	**1.66**
Si(2) – O	**1.63**	**1.65**	**1.62**	**1.64**	**1.61**
Si(3) – O	**1.63**	**1.61**	**1.60**	**1.62**	**1.62**

Table 5. Selected bond angles in $Ca_3RE_2(Si_3O_9)_2$ (RE= Yb, Dy, Gd, Sm, Nd).

Bond angles (°)	Yb	Dy	Gd	Sm	Nd
O(1) – Si(1) – O(2)	119.4	117.3	119.6	114.2	114.9
O(1) – Si(1) – O(4)	119.1	119.1	118.1	123.7	119.5
O(1) – Si(1) – O(5)	114.0	109.4	110.1	106.8	106.8
O(2) – Si(1) – O(4)	97.5	101.0	99.6	103.3	104.9
O(2) – Si(1) – O(5)	104.7	106.1	105.6	101.9	104.6
O(4) – Si(1) – O(5)	99.0	102.3	101.7	104.4	104.8
O – Si(1) – O	**109.0**	**109.2**	**109.1**	**109.1**	**109.3**
O(3) – Si(2) – O(5)	98.4	98.8	102.4	104.1	101.7
O(3) – Si(2) – O(6)	121.1	123.2	117.4	120.7	126.7
O(3) – Si(2) – O(7)	105.9	105.1	104.9	104.8	103.9
O(5) – Si(2) – O(6)	113.1	110.9	112.4	109.6	109.9
O(5) – Si(2) – O(7)	105.2	108.1	106.1	105.8	104.4
O(6) – Si(2) – O(7)	111.4	109.6	112.5	110.6	108.1
O – Si(2) – O	**109.2**	**109.3**	**109.3**	**109.3**	**109.1**
O(2) – Si(3) – O(7)	111.1	106.8	104.3	103.2	107.3
O(2) – Si(3) – O(8)	103.4	101.1	101.3	103.9	98.5
O(2) – Si(3) – O(9)	108.6	112.8	112.2	113.1	108.0
O(7) – Si(3) – O(8)	102.0	105.8	102.6	105.8	108.7
O(7) – Si(3) – O(9)	109.2	106.9	106.2	108.2	114.6
O(8) – Si(3) – O(9)	122.1	122.3	126.0	121.1	118.1
O – Si(3) – O	**109.4**	**109.3**	**108.8**	**109.2**	**109.2**

Table 6. $(Ca/RE)_1$, $(Ca/RE)_2$ and $(Ca/RE)_3$ site occupancies for $Ca_3RE_2(Si_3O_9)_2$ (RE= Yb, Dy, Gd, Sm, Nd).

Site occupancies	Yb	Dy	Gd	Sm	Nd
$(Ca/RE)_1$	0.89/0.11	0.82/0.18	0.79/0.21	0.75/0.25	0.71/0.29
$(Ca/RE)_2$	0.55/0.45	0.56/0.44	0.57/0.43	0.56/0.44	0.58/0.42
$(Ca/RE)_3$	0.15/0.85	0.21/0.79	0.27/0.73	0.29/0.71	0.38/0.62